



1 Upper limits on $gg \rightarrow H \rightarrow W^+W^-$ and constraints on the Higgs boson mass in
2 fourth-generation fermion models from single lepton + \cancel{E}_T + jets final states

3 The DØ Collaboration
4 URL <http://www-d0.fnal.gov>
5 (Dated: April 25, 2011)

We report results from searches for the standard model Higgs boson in the presence of a heavy, sequential fourth generation of fermions using 5.4 fb^{-1} of integrated luminosity in $p\bar{p}$ collisions at $\sqrt{s} = 1.96 \text{ TeV}$ collected with the D0 detector at the Fermilab Tevatron Collider. This analysis considers decay channels $gg \rightarrow H \rightarrow W^+W^- \rightarrow \ell\nu q'q$, where $\ell = (e \text{ or } \mu)$ with final states containing a single charged lepton, two or more jets, and missing transverse energy and is also sensitive to decays $H \rightarrow ZZ \rightarrow \ell\ell qq$ where one lepton (ℓ) is not identified. The 95% C.L. upper limit on $\sigma(gg \rightarrow H) \times B(H \rightarrow WW(ZZ))$ is 1.69, 2.60, 0.74 pb at $M_H = 165, 200, 250 \text{ GeV}$, respectively. Assuming the presence of a fourth sequential generation of fermions with large masses, we exclude at the 95% C.L. a standard-model-like Higgs boson with a mass between 159 and 183 GeV.

I. INTRODUCTION

The phenomena of electroweak symmetry-breaking is described in the standard model (SM) by introducing complex scalar fields that interact with the massless electroweak gauge fields. Spontaneous symmetry breaking of the fields according to the Higgs mechanism [1–3] generates masses for the W and Z bosons. Fits to precision electroweak data favor a low mass Higgs with $M_H \lesssim 2M_W$, but the presence of an additional generation of fermions can extend the consistency of these fits up to ~ 300 GeV [4], where any fourth-generation extension to the SM is required to have a mass $m_{\nu_4} > M_Z/2$ to satisfy constraints from the observed width of the Z boson [5]. This note presents a search for the production of Higgs bosons via gluon fusion with subsequent decay to $WW(ZZ)$ having only one (identified) charged lepton in the final state. Our analysis is most sensitive to final-state topologies with a single charged lepton (e or μ), two or more jets, and missing transverse energy (\cancel{E}_T), arising from $H \rightarrow W^+W^- \rightarrow \ell\nu q'q$ decays. Smaller signal contributions from $H \rightarrow ZZ \rightarrow \ell\cancel{\ell}qq$, where $\cancel{\ell}$ represents an unidentified lepton, and $H \rightarrow W^+W^- \rightarrow \tau\nu q'q$ with $\tau \rightarrow \ell\nu\nu$ are also considered. This analysis extends the channels used in previous Tevatron limits [6] on Higgs boson production in the presence of heavy fourth-generation fermions. Because of the large branching fractions for mixed leptonic and hadronic final states and also reduced background for final states with highly boosted W bosons, this channel can achieve comparable sensitivities to considering fully leptonic decays of the Higgs boson for the highest masses accessible at the Tevatron energies.

The existence of additional fermions modifies both the production and decay properties of the Higgs boson. The ggH coupling is enhanced by roughly a factor $K_e \approx 3$ relative to the SM coupling [4, 7, 8], enhancing the production cross section by a factor of $K_e^2 \approx 9$. However, for $M_H \approx 300$ GeV, this factor is reduced to approximately 7.5 with asymptotically large masses for the fourth-generation quarks, due to increased contributions from the standard model top quark as M_H approaches $2m_t$. Although the partial decay width for $H \rightarrow gg$ is enhanced by the same factor as the production cross section, $H \rightarrow W^+W^-$ decay continues to dominate over these loop-mediated decays for $M_H > 135$ GeV. We consider the production of Higgs bosons only via gluon fusion with two scenarios for heavy fourth-generation fermions, a “low-mass” scenario with $m_{\nu_4} = 80$ GeV and $m_{\ell_4} = 100$ GeV and a “high-mass” scenario with $m_{\nu_4} = m_{\ell_4} = 1$ TeV. The low-mass scenario is chosen to satisfy experimental constraints and to have maximum impact on the Higgs boson decay branching ratios. In the high-mass scenario the decay branching ratios of the Higgs boson are not affected. In both scenarios the mass of the fourth-generation down-type quark is set to $m_{d_4} = 400$ GeV and that of the up-type quark is set to $m_{u_4} = 450$ GeV.

II. DATA AND SIMULATED SAMPLES

The D0 collaboration has previously searched for the standard model Higgs boson in final states containing a single charged lepton, two or more jets, and missing transverse energy [9] using a data sample of 5.4 fb^{-1} of integrated luminosity. This analysis uses the same data set evaluated in the context of an additional, fourth-generation, family of heavy fermions. The primary backgrounds are from V +jets ($V = W$ or Z), top quark, diboson production, and multijet (MJ) events containing a lepton or lepton-like signature with \cancel{E}_T generally arising from mismeasurement of jet energies.

The D0 detector [10–12] consists of tracking, calorimetric and muon detectors. Charged particle tracks are reconstructed using silicon microstrip (SMT) detectors and a scintillating fiber tracker, within a 1.9 T solenoid. Three uranium/liquid-argon calorimeters measure particle energies that are reconstructed into hadronic jets using an iterative midpoint cone algorithm with a cone radius of 0.5 [13]. Electrons and muons are identified through association of charged particle tracks with clusters in the electromagnetic sections of the calorimeters or with hits in the muon detector, respectively. We obtain the \cancel{E}_T from a vector sum of transverse components of calorimeter energy depositions and correct it for identified muons. Jet energies are calibrated using transverse momentum balance in photon+jet events [14], and the correction is propagated to the \cancel{E}_T . The data are recorded using triggers designed to select single electrons or muons and also a combination of an electron and jets. After imposing data quality requirements, the total integrated luminosity is 5.4 fb^{-1} [15].

Background contributions from most SM processes are determined through Monte Carlo (MC) simulation, with normalizations constrained by data, while the multijet background is estimated from data. The dominant background is from V +jets processes, which are generated with ALPGEN [16]. The transverse momentum (p_T) spectrum of the Z boson in the MC is reweighted to match that observed in data [17]. The p_T spectrum of the W boson is reweighted using the same dependence, but corrected for differences between the p_T spectra of Z and W bosons predicted in next-to-next-to-leading order (NNLO) QCD [18]. Backgrounds from $t\bar{t}$ and electroweak single top-quark production are simulated using the ALPGEN and COMPHEP [19] generators, respectively. Vector boson pair production and Higgs boson signals are generated with PYTHIA [20]. All these simulations use CTEQ6L1 parton distribution functions (PDF) [21, 22]. Both ALPGEN and COMPHEP samples are interfaced with PYTHIA for modeling of parton evolution

and hadronization.

Relative normalizations for the various V +jets processes are obtained from calculations of cross sections at next-to-leading order using MCFM [23], while the absolute normalization for the total V +jets background is constrained through a comparison to data, following the subtraction of other background sources. This increases the normalization of the background from V +jets by about 2%, compared with the expectation from ALPGEN after scaling to the total cross sections calculated at NNLO [24] with the MRST2004 NNLO PDFs [25]. Cross sections for other SM backgrounds are taken from Ref. [26–28], or calculated with MCFM, and those for signal are taken from Ref. [8]. The branching ratios for $B(H \rightarrow WW(ZZ))$ are calculated using HDECAY modified to include fourth-generation fermions [4]. The p_T spectra for diboson events in background are corrected to match those of the MC@NLO generator [29]. The p_T spectra from the contribution of gluon fusion to the Higgs boson signal, as generated in PYTHIA, are modified to match those obtained from HqT [30, 31].

Signal and background events from MC are passed through a full GEANT3-based simulation [32] of detector response, and then processed with the same reconstruction program as used for data. Events from randomly selected beam crossings, corresponding to the same instantaneous luminosity profile as data, are overlaid on the simulated events to model detector noise and contributions from the presence of additional $p\bar{p}$ interactions. Parameterizations of trigger efficiency for leptons are determined using $Z \rightarrow \ell\ell$ decays [33]. Any remaining differences between data and simulation in the reconstruction of electrons, muons, and jets are adjusted in simulated events to match those observed in data, and these corrections are also propagated to the \cancel{E}_T .

III. EVENT SELECTION

Events are selected to contain candidates for $W \rightarrow \ell\nu$ decay by requiring $\cancel{E}_T > 15$ GeV and the presence of a lepton with $p_T > 15$ GeV that is isolated relative to jets, namely located outside jet cones $\Delta R(\ell, j) > 0.5$, with $(\Delta R)^2 = (\phi^\ell - \phi^j)^2 + (\eta^\ell - \eta^j)^2$, where ϕ^x and η^x are the azimuth and pseudorapidity [34] of object x . The position of the $p\bar{p}$ interaction vertex (PV) along the beam direction (z_{PV}) is required to be reconstructed within the longitudinal acceptance of the SMT, $|z_{PV}| < 60$ cm. The lepton is required to originate from the PV and to pass more restrictive isolation criteria based on tracking information and energy deposited near its trajectory in the calorimeter. Electrons must also satisfy criteria on the spatial distributions of their showers, and timing criteria is used to reject cosmic-ray background in events with muons. Electrons and muons are required to be located within $|\eta_{det}| < 1.1$ and < 1.6 , respectively, where η_{det} is the pseudorapidity assuming the object originates from the center of the detector. To reduce background from $Z \rightarrow \ell\ell$, top quark, and diboson events, and to assure selected events do not overlap with those used in the $H \rightarrow WW \rightarrow \ell\nu\ell'\nu'$ analysis channels, we veto any event containing a second charged lepton satisfying less stringent identification criteria. We also require at least two jets with $|\eta^j| < 2.5$ and $p_T > 20$ GeV that contain associated tracks originating from the PV. The leading two jets are used to reconstruct the W boson decaying to $q'q$. To estimate the MJ background, we use data samples orthogonal to our signal sample, where isolation requirements on the leptons are reversed to create a sample of lepton candidates that are dominated by MJ events. Additional details on event selections are given in Ref. [9]. Event yields in data and those expected for signal and background are shown in Table I.

TABLE I: Number of signal and background events expected after selection requirements. Expected signal yields are shown for $M_H = 200$ GeV and the three values listed correspond to SM and low and high mass fourth-generation models. For backgrounds, “Top” includes pair and single top-quark production and “ VV ” includes all non-resonant diboson processes. The overall background normalization is fixed to the data by adjusting the V +jets cross sections.

Channel	$gg \rightarrow H$			V +jets	Multijet	Top	VV	Total Background	Data
	SM	4G (low mass)	4G (high mass)						
Electron	23.8	174.8	197.4	52158	11453	2433	1584	67627	67627
Muon	17.0	123.5	139.4	46842	2720	1598	1273	52433	52433

IV. MULTIVARIATE ANALYSIS

We use a random forest (RF) classifier [35–37], trained on a randomly selected collection of signal and background MC events as well as MJ events from data, to separate signal from background. The RF examines a set of about 30 discriminating variables formed from particle 4-vectors, angles between these vectors, and combinations of kinematic variables such as reconstructed masses and event shapes. An RF is trained separately for electron and muon channels

101 using signal hypotheses for $115 < M_H < 300$ GeV in steps of 5(10) GeV for M_H below (above) 200 GeV. The outputs
 102 of the final RF discriminants combined for both lepton channels, for $M_H = 200$ GeV, are shown in Fig. 1 for the low-
 103 mass fourth-generation fermion scenario. Agreement is observed with expectations from SM background, and these
 104 RF-outputs are therefore used to set upper limits on the cross section for Higgs production in the two fourth-generation
 105 fermion scenarios.

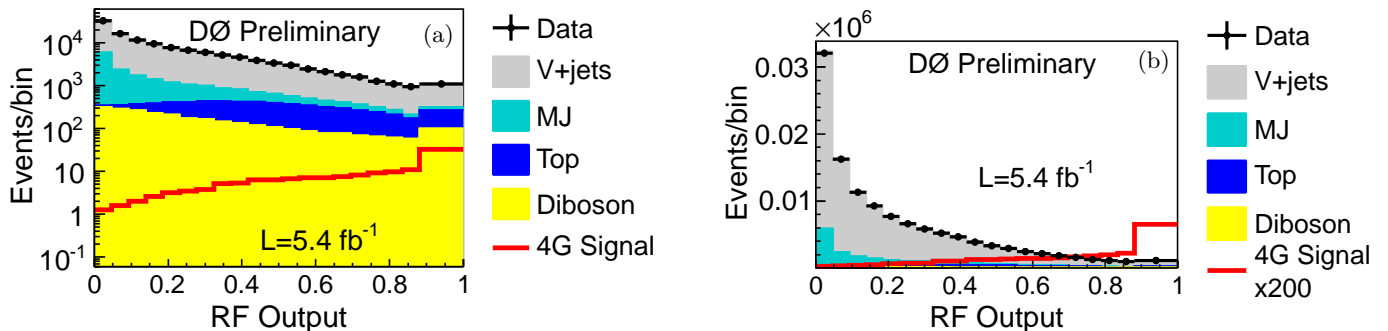


FIG. 1: The outputs of the final RF discriminants combined for both lepton channels for data, different backgrounds, and signal expectations for $M_H = 200$ GeV in the low-mass fourth-generation fermion scenario. The distributions are shown in (a) logarithmic and (b) linear scales.

V. SYSTEMATIC UNCERTAINTIES

107 Systematic uncertainties affect the normalizations and distributions of the final discriminants and are therefore
 108 included in the determination of limits. These arise from a variety of sources, and their impact is assessed by changing
 109 each input discriminant to the RF by ± 1 standard deviation. The most significant uncertainties are from calibration
 110 of jet energies (0.7–6%), jet resolution (0.5–3%), efficiency of jet reconstruction (0.5–4%), that of lepton identification
 111 and modeling of the trigger (4%), estimation of the multijet background (6.5–26%), and integrated luminosity (6.1%).
 112 Theoretical uncertainties on cross sections for backgrounds are taken from Ref. [23, 26–28]. The uncertainties on
 113 cross sections for signal are taken from Ref. [8, 38–41]. Because the overall cross section for V +jets production
 114 is constrained by data, the uncertainty on its normalization is anticorrelated with MJ background. The impact of
 115 theoretical uncertainties on distributions of the final discriminants are assessed by varying a common renormalization
 116 and factorization scale, by comparing ALPGEN interfaced with HERWIG [42] to ALPGEN interfaced with PYTHIA for
 117 V +jets samples, and by varying the PDF parameters used to generate the MC samples, following the prescription of
 118 Ref. [21, 22].

VI. LIMIT SETTING PROCEDURE

120 Upper limits on the production cross section multiplied by branching fractions are determined using the modified
 121 frequentist CL_S approach [43, 44]. A test statistic based on the logarithm of the ratio of likelihoods (LLR) [43, 44]
 122 for the data to represent signal+background and background-only hypotheses is summed over all bins of the final
 123 discriminant from each of the lepton decay channels. To minimize degradation in sensitivity, scaling factors for the
 124 systematic uncertainties are fitted to the data by maximizing a likelihood function for both the signal+background
 125 and background-only hypotheses, with the systematic uncertainties constrained through Gaussian priors on their
 126 probabilities [45]. Correlations among systematic uncertainties in signal and background are taken into account in
 127 extracting the final results. Figure 2 shows the combined background-subtracted data and the uncertainties on the
 128 RF discriminant for background after the fit to data. Also shown is the expectation for the contribution from signal
 129 in the low-mass fourth-generation fermion model for $M_H = 165$ and 200 GeV. No significant excess is observed in the
 130 data.

VII. RESULTS

132 When setting limits on $\sigma(gg \rightarrow H) \times B(H \rightarrow WW(ZZ))$, we do not include the theoretical uncertainty on the
 133 prediction of $\sigma(gg \rightarrow H) \times B(H \rightarrow WW(ZZ))$ in the fourth-generation models since these limits are independent of

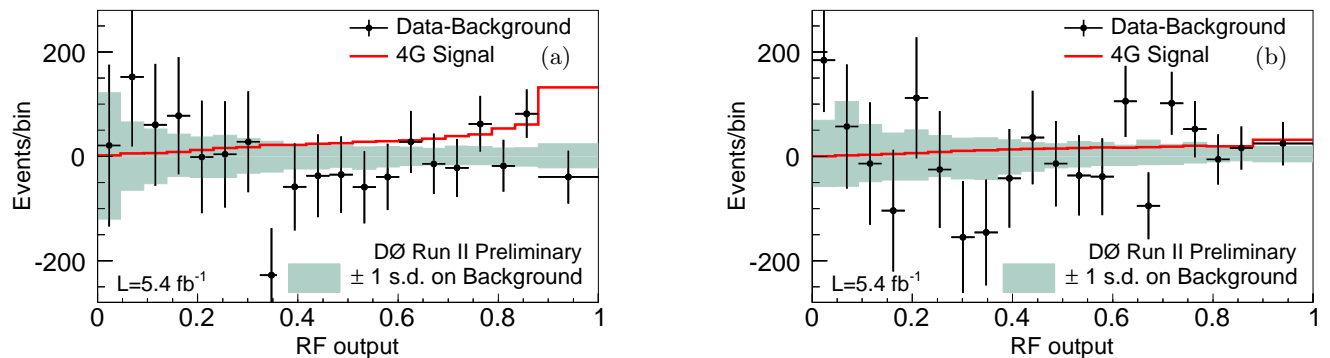


FIG. 2: The combined background-subtracted data and one standard deviation (s.d.) uncertainty on total background after applying constraints on systematic uncertainties through fits to data along with the expected Higgs signal assuming the low-mass fourth-generation fermion scenario for (a) $M_H = 165$ GeV and (b) $M_H = 200$ GeV.

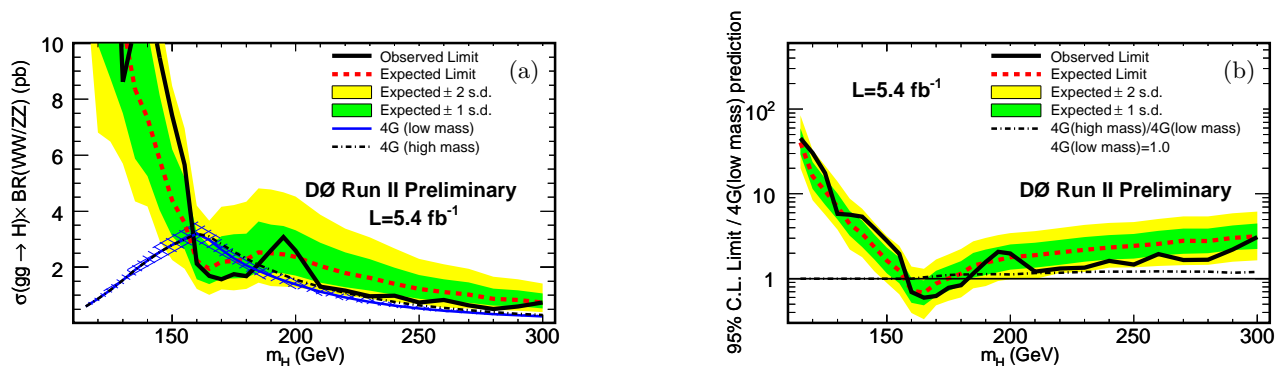


FIG. 3: The (a) combined observed (solid black lines) and median expected (dashed black lines) 95% C.L. upper limits on $\sigma(gg \rightarrow H) \times B(H \rightarrow WW(ZZ))$. The shaded bands indicate the ± 1 standard deviation (s.d.) and ± 2 s.d. intervals on the distribution of the limits that are expected if a Higgs boson signal is not present. Also shown on each graph is the prediction for a fourth-generation model in the low-mass and high-mass scenarios, 4G (Low mass) and 4G (High mass) respectively. The hatched areas indicate the theoretical uncertainty from PDF and scale uncertainties. The dot-dashed curves show the high-mass theoretical prediction. Figure (b) shows the 95% C.L. combined limit relative to the low-mass theoretical prediction, where the uncertainties in the signal prediction are included in the limit. Also shown in Fig. (b) is the prediction of the signal rate in the high-mass scenario, divided by that of the low-mass scenario.

134 the predictions. For setting limits on M_H in the context of fourth-generation models, we include the uncertainties
 135 on the theoretical predictions as described below. The limits on $\sigma(gg \rightarrow H) \times B(H \rightarrow WW(ZZ))$ for electron and
 136 muon channels combined are shown in Fig. 3(a) along with the fourth-generation theory predictions for the high-
 137 mass and low-mass scenarios. The uncertainty bands shown on the low-mass theoretical prediction are the sum in
 138 quadrature of the MSTW 2008 [46] 90% C.L. parton distribution function (PDF) uncertainties and the factorization
 139 and renormalization scale uncertainties from Table 1 of Ref. [8]. The scale uncertainties are independent of M_H and
 140 are similar to the uncertainties for SM $\sigma(gg \rightarrow H)$ predictions [8, 38–41]. The PDF uncertainties, however, grow with
 141 increasing M_H , as gluons carrying larger momentum fractions in the proton are required to produce more massive
 142 Higgs bosons.

143 In order to set limits on M_H in these two scenarios, we perform a second combination, including the uncertainties
 144 on the theoretical predictions of $\sigma(gg \rightarrow H) \times B(H \rightarrow WW(ZZ))$ due to scale and PDF uncertainties at each tested
 145 value of M_H . The resulting ratio of limits are computed relative to the model prediction, and are shown in Fig. 3(b)
 146 for the low-mass scenario, which gives the smaller excluded range of M_H in comparison to the high-mass case. In
 147 this scenario, we exclude at the 95% C.L. a SM-like Higgs boson with a mass in the range 159 – 183 GeV. Using
 148 the median limits on $\sigma(gg \rightarrow H) \times B(H \rightarrow WW(ZZ))$, from an ensemble of pseudo-experiments in the absence of
 149 a signal, to quantify the sensitivity, we expect to exclude the mass range 157 – 175 GeV. In the high-mass scenario,
 150 which predicts a larger $B(H \rightarrow W^+W^-)$ at high M_H than that predicted in the low-mass scenario, we exclude at
 151 the 95% C.L. the mass range 159 – 184 GeV and expect to exclude the mass range 157 – 179 GeV. Table II gives
 152 cross section limits for the two scenarios. The sensitivity of this leptonic plus hadronic decay channel is found to be

153 comparable to that using fully leptonic decays for $M_H \gtrsim 250$ GeV.

TABLE II: The observed and median expected 95% C.L. upper limits on $\sigma(gg \rightarrow H) \times B(H \rightarrow WW(ZZ))$ for M_H between 115 GeV and 300 GeV for predictions of the low-mass and the high-mass fourth-generation scenarios discussed in the text. All limits are presented in pb.

M_H GeV	Low-mass limits				High-mass limits			
	Obs.	Ratio (Obs./4Gen)	Exp.	Ratio (Exp./4Gen)	Obs.	Ratio (Obs./4Gen)	Exp.	Ratio (Exp./4Gen)
115	25.88	43.35	24.01	40.22	26.2	43.88	24.15	40.45
120	25.14	28.84	13.97	16.02	25.05	28.73	13.91	15.96
125	19.96	16.71	12.48	10.45	20	16.75	12.29	10.29
130	8.62	5.58	10.72	6.94	8.96	5.80	10.55	6.83
135	10.58	5.57	8.35	4.39	10.48	5.51	8.2	4.31
140	11.64	5.20	7.32	3.27	11.57	5.17	7.33	3.27
145	9.48	3.74	5.83	2.30	9.57	3.77	5.7	2.25
150	7.41	2.66	4.4	1.58	7.43	2.66	4.37	1.57
155	5.65	1.88	3.59	1.20	5.63	1.88	3.63	1.21
160	2.13	0.66	2.22	0.69	2.1	0.66	2.2	0.69
165	1.69	0.57	1.94	0.65	1.68	0.54	1.94	0.63
170	1.57	0.60	2.2	0.84	1.59	0.56	2.21	0.78
175	1.76	0.76	2.22	0.96	1.7	0.67	2.24	0.88
180	1.68	0.81	2.28	1.10	1.58	0.69	2.28	0.99
185	2.1	1.12	2.53	1.36	2.11	1.01	2.54	1.22
190	2.6	1.54	2.5	1.48	2.63	1.39	2.51	1.32
195	3.07	2.01	2.46	1.61	2.85	1.66	2.46	1.43
200	2.6	1.88	2.37	1.71	2.6	1.66	2.39	1.53
210	1.3	1.16	2.04	1.82	1.3	1.00	2.04	1.57
220	1.16	1.26	1.8	1.96	1.15	1.06	1.76	1.63
230	0.97	1.28	1.62	2.14	0.97	1.07	1.63	1.80
240	0.98	1.55	1.41	2.23	0.97	1.27	1.4	1.84
250	0.74	1.39	1.23	2.31	0.73	1.13	1.23	1.91
260	0.83	1.83	1.12	2.47	0.84	1.53	1.13	2.06
270	0.64	1.65	1.03	2.66	0.59	1.26	1.04	2.23
280	0.51	1.53	0.87	2.61	0.52	1.30	0.88	2.20
290	0.6	2.08	0.83	2.88	0.58	1.68	0.81	2.35
300	0.74	2.95	0.74	2.95	0.72	2.41	0.75	2.51

Acknowledgments

We thank the staffs at Fermilab and collaborating institutions, and acknowledge support from the Department of Energy and National Science Foundation (USA), Commissariat à l’Energie Atomique and CNRS/Institut National de Physique Nucléaire et de Physique des Particules (France), Ministry of Education and Science, Agency for Atomic Energy and RF President Grants Program (Russia), CAPES, CNPq, FAPERJ, FAPESP and FUNDUNESP (Brazil), Departments of Atomic Energy and Science and Technology (India), Colciencias (Colombia), CONACyT (Mexico), KRF (Korea), CONICET and UBACyT (Argentina), The Foundation for Fundamental Research on Matter (The Netherlands), PPARC (United Kingdom), Ministry of Education (Czech Republic), Natural Sciences and Engineering Research Council and WestGrid Project (Canada), BMBF (Germany), A.P. Sloan Foundation, Civilian Research and Development Foundation, Research Corporation, Texas Advanced Research Program, and the Alexander von Humboldt Foundation.

-
- [1] P. W. Higgs, *Phys. Lett.* **12**, 132 (1964).
 [2] P. W. Higgs, *Phys. Rev. Lett.* **13**, 508 (1964).
 [3] P. W. Higgs, *Phys. Rev.* **145**, 1156 (1966).
 [4] G. D. Kribs, T. Plehn, M. Spannowsky, and T. M. P. Tait, *Phys. Rev.* **D76**, 075016 (2007), 0706.3718.
 [5] ALEPH, DELPHI, L3, OPAL, SLD, J. A. Bagger *et al.*, *Phys. Rept.* **427**, 257 (2006), hep-ex/0509008.
 [6] CDF and D0 Collaboration, T. Aaltonen *et al.*, *Phys. Rev. D* **82**, 011102 (2010).
 [7] E. Arik, O. Cakir, S. A. Cetin, and S. Sultansoy, *Acta Phys. Polon.* **B37**, 2839 (2006), hep-ph/0502050.
 [8] C. Anastasiou, R. Boughezal, and E. Furlan, *JHEP* **06**, 101 (2010), 1003.4677.
 [9] D0 Collaboration, V. M. Abazov *et al.*, (2011), 1101.6079.
 [10] D0 Collaboration, V. M. Abazov *et al.*, *Nucl. Instrum. Meth.* **A565**, 463 (2006), physics/0507191.
 [11] M. Abolins *et al.*, *Nucl. Instrum. Meth.* **A584**, 75 (2008), 0709.3750.
 [12] D0 Collaboration, R. Angstadt *et al.*, *Nucl. Instrum. Meth.* **A622**, 298 (2010), 0911.2522.
 [13] G. C. Blazey *et al.*, (2000), hep-ex/0005012.
 [14] D0 Collaboration, V. M. Abazov *et al.*, *Phys. Rev. Lett.* **101**, 062001 (2008), 0802.2400.
 [15] D0 Run II, T. Andeen *et al.*, FERMILAB-TM-2365.
 [16] M. L. Mangano, M. Moretti, F. Piccinini, R. Pittau, and A. D. Polosa, *JHEP* **07**, 001 (2003), hep-ph/0206293.
 [17] D0 Collaboration, V. M. Abazov *et al.*, *Phys. Rev. Lett.* **100**, 102002 (2008), 0712.0803.
 [18] K. Melnikov and F. Petriello, *Phys. Rev.* **D74**, 114017 (2006), hep-ph/0609070.
 [19] CompHEP, E. Boos *et al.*, *Nucl. Instrum. Meth.* **A534**, 250 (2004), hep-ph/0403113.
 [20] T. Sjostrand, S. Mrenna, and P. Z. Skands, *JHEP* **05**, 026 (2006), hep-ph/0603175.
 [21] J. Pumplin *et al.*, *JHEP* **07**, 012 (2002), hep-ph/0201195.
 [22] D. Stump *et al.*, *JHEP* **10**, 046 (2003), hep-ph/0303013.
 [23] J. M. Campbell and R. K. Ellis, *Phys. Rev.* **D60**, 113006 (1999), hep-ph/9905386.
 [24] R. Hamberg, W. L. van Neerven, and T. Matsuura, *Nucl. Phys.* **B359**, 343 (1991), Erratum: *ibid.* vol B644, p 403 (2002).
 [25] A. D. Martin, R. G. Roberts, W. J. Stirling, and R. S. Thorne, *Phys. Lett.* **B604**, 61 (2004), hep-ph/0410230.
 [26] M. Cacciari, S. Frixione, M. L. Mangano, P. Nason, and G. Ridolfi, *JHEP* **04**, 068 (2004), hep-ph/0303085.
 [27] N. Kidonakis and R. Vogt, *Phys. Rev.* **D68**, 114014 (2003), hep-ph/0308222.
 [28] N. Kidonakis, *Phys. Rev.* **D74**, 114012 (2006), hep-ph/0609287.
 [29] S. Frixione and B. R. Webber, *JHEP* **06**, 029 (2002), hep-ph/0204244.
 [30] G. Bozzi *et al.*, *Phys. Lett.* **B 564**, 65 (2003), 0302104.
 [31] G. Bozzi *et al.*, *Nucl. Phys.* **B 737**, 73 (2006), 0508068.
 [32] R. Brun and F. Carminati, GEANT Detector Description and Simulation Tool, CERN Program Library Long Writeup W5013, unpublished, 1993.
 [33] D0 Collaboration, V. M. Abazov *et al.*, *Phys. Rev.* **D76**, 012003 (2007), hep-ex/0702025.
 [34] The pseudorapidity is defined as $\eta = -\ln[\tan(\theta/2)]$, where θ is the polar angle with respect to the proton beam direction.
 [35] L. Breiman, *Mach. Learn.* **45**, 5 (2001).
 [36] I. Narsky, (2005), arXiv:physics/0507143 [physics.data-an].
 [37] I. Narsky, (2005), arXiv:physics/0507157 [physics.data-an].
 [38] D. de Florian and M. Grazzini, *Phys. Lett.* **B674**, 291 (2009), 0901.2427.
 [39] T. Hahn, S. Heinemeyer, F. Maltoni, G. Weiglein, and S. Willenbrock, (2006), hep-ph/0607308.
 [40] J. Baglio and A. Djouadi, *JHEP* **10**, 064 (2010), 1003.4266.
 [41] A. Djouadi, J. Kalinowski, and M. Spira, *Comput. Phys. Commun.* **108**, 56 (1998), hep-ph/9704448.
 [42] G. Corcella *et al.*, *JHEP* **01**, 010 (2001), hep-ph/0011363.
 [43] T. Junk, *Nucl. Instrum. Meth.* **A434**, 435 (1999), hep-ex/9902006.
 [44] A. L. Read, *J. Phys.* **G28**, 2693 (2002).
 [45] W. Fisher, Systematics and limit calculations, FERMILAB-TM-2386-E.

²¹¹ [46] A. D. Martin, W. J. Stirling, R. S. Thorne, and G. Watt, *Eur. Phys. J.* **C64**, 653 (2009), 0905.3531.